Construction and Building Materials 49 (2013) 974–984

Contents lists available at SciVerse ScienceDirect

Construction and Building Materials

journal homepage: www.elsevier.com/locate/conbuildmat

Serviceability flexural ductility of FRP RC beams: A discrete rotation approach

Deric John Oehlers [a,*], Rahimah Muhamad [b], M.S. Mohamed Ali [a]

[a] School of Civil, Environmental and Mining Engineering, University of Adelaide, South Australia 5005, Australia
[b] UTM Razak School of Engineering and Advanced Technology, Universiti Teknologi Malaysia International Campus, Kuala Lumpur 54100, Malaysia

HIGHLIGHTS

- Closed form solutions for quantifying concentrations of rotation at serviceability.
- A mechanics based discrete rotation approach for quantifying deflection.
- Can cope with any type of FRP reinforcement with any type of bond characteristic.
- Can also predict gradual development of cracks and their widening and spacing.
- Precursor of hinge development.

ARTICLE INFO

Article history:
Available online 17 November 2012

Keywords:
Deflection
FRP reinforcement
FRP reinforcing bars
Serviceability
RC beams
RC slabs
RC bond

ABSTRACT

Flexural ductility in reinforced concrete members may be defined as concentrations of rotation at discrete points. As such, flexural ductility affects the serviceability deflection of RC beams once flexural cracking, in which there is a discrete rotation between the crack faces, has occurred and which is the subject of this paper. Design rules for quantifying the deflection of steel reinforced RC beams and slabs are generally based on a full-interaction moment–curvature (M/χ) approach that requires the flexural rigidity to be calibrated empirically. Being empirically based, these design rules should only be applied within the bounds of the tests from which they were derived that is for steel reinforcement in which the modulus is fairly constant and with ribbed bars which have a very good bond with the concrete. These bounds do not apply to FRP reinforcing bars where the modulus can vary enormously depending on the type and density of fibre and where the bond between the FRP reinforcement and concrete can also vary widely depending on the manufacturing process. Hence it is both difficult and expensive to quantify empirically, using the M/χ approach, the deflection of RC beams with FRP reinforcement due to the very wide range of these variables. In this paper, an alternative mechanics based discrete rotation approach for the non-time dependent deflection is developed for FRP reinforced flexural members and which is validated by FRP RC beam tests. Being mechanics based, this discrete rotation approach can cope with any type of FRP reinforcing bar with any type of bond characteristic. As with the M/χ approach, the material properties are determined by tests but unlike the M/χ approach in which the flexural rigidity, which is a major component of the model, has to be calibrated through tests, no component of this discrete-rotation model has to be determined experimentally. As this is a generic approach and can be used for any type of reinforcement and bond, this mechanics approach should speed up the development of new FRP products and the development of accurate design rules for deflection for these new FRP products.

© 2012 Elsevier Ltd. All rights reserved.

1. Introduction

The use of FRP reinforcing bars in reinforced concrete flexural members is gaining wider acceptance in reinforced concrete due in particular to the corrosion resistance properties of the FRP reinforcement [1–7]. This has necessitated as part of the design process the need for quantifying the deflection of these members [8,9]. Much of the research on quantifying the deflection of RC members has used as a starting point the design rules for steel reinforced RC beams or slabs which are based on effective flexural rigidities that can only be determined empirically [10–13]. Being empirically based they are limited to the bounds of the tests from which they were calibrated, which in general is a reinforcing bar of a high and constant elastic modulus and with very good bond between the reinforcement and the concrete. This in effect precludes the direct

* Corresponding author. Tel.: +61 8 8303 4314; fax: +61 8 8303 4359.
E-mail address: doehlers@civeng.adelaide.edu.au (D.J. Oehlers).

0950-0618/$ - see front matter © 2012 Elsevier Ltd. All rights reserved.
http://dx.doi.org/10.1016/j.conbuildmat.2012.10.001

Nomenclature

A_r	cross-sectional area of FRP reinforcing bar
A_c	cross-sectional of concentrically loaded prism
d	depth of beam
d_{pri}	depth of prism
E_r	modulus of FRP reinforcing bar
E_c	modulus elasticity of concrete
F	load in reinforcing bar
$F_{li\text{-}pr}$	load to induce primary crack based on τ–δ linear ascending
$F_{li\text{-}sec}$	load to induce secondary crack based on τ–δ linear ascending
$F_{li\text{-}ter}$	load to induce tertiary crack based on τ–δ linear ascending
$F_{pa\text{-}pr}$	load to induce primary crack based on τ–δ parabolic ascending
$F_{pa\text{-}sec}$	load to induce secondary crack based on τ–δ parabolic ascending
$F_{pa\text{-}ter}$	load to induce tertiary crack based on τ–δ parabolic ascending
f_{ct}	tensile strength of the concrete
$(L_{cr})_{pr}$	length of primary crack region
$(L_{cr})_{sec}$	length of secondary cracks region
L_u	length of uncracked region
L_p	perimeter length of FRP bar
M_{app}	applied moment
M_{pr}	moment to cause a primary cracks
M_{sec}	moment to cause a secondary cracks
M_{serv}	serviceability moment
P_c	concrete force
P_r	reinforcement force
$P_{li\text{-}\infty}$	force in reinforcing bar for infinitely long element based on τ–δ of linear ascending
$P_{li\text{-}sp}$	force in reinforcing bar for element length S_p based on τ–δ of linear ascending
$P_{li\text{-}sp/2}$	force in reinforcing bar for element length $S_p/2$ based on τ–δ of linear ascending
$P_{li\text{-}sp/4}$	force in reinforcing bar for element length $S_p/4$ based on τ–δ of linear ascending
$P_{pa\text{-}\infty}$	force in reinforcing bar for infinitely long element based on τ–δ of parabolic ascending
$P_{pa\text{-}sp}$	force in reinforcing bar for element length S_p based on τ–δ of parabolic ascending
$P_{pa\text{-}sp/2}$	force in reinforcing bar for element length $S_p/2$ based on τ–δ of parabolic ascending
$P_{pa\text{-}sp/4}$	force in reinforcing bar for element length $S_p/4$ based on τ–δ of parabolic ascending
$S_{li\text{-}pr}$	primary crack spacing for element length S_p based on τ–δ of linear ascending
$S_{li\text{-}sec}$	secondary crack spacing for element length $S_p/2$ based on τ–δ of linear ascending
$S_{li\text{-}ter}$	tertiary crack spacing for element length $S_p/4$ based on τ–δ of linear ascending
$S_{pa\text{-}pr}$	primary crack spacing for element length S_p based on τ–δ of parabolic ascending
$S_{pa\text{-}sec}$	secondary crack spacing for element length $S_p/2$ based on τ–δ of parabolic ascending
$S_{pa\text{-}ter}$	tertiary crack spacing for element length $S_p/4$ based on τ–δ of parabolic ascending
w_{cr}	width of the crack at the level of the reinforcement
τ_{max}	peak shear stress
$\Delta_{li\text{-}\infty}$	slip at crack face for infinitely long element based on τ–δ of linear ascending
$\Delta_{li\text{-}sp}$	slip at crack face for element length S_p based on τ–δ of linear ascending
$\Delta_{li\text{-}sec}$	slip at crack face for element length $S_p/2$ based on τ–δ of linear ascending
$\Delta_{li\text{-}ter}$	slip at crack face for element length $S_p/4$ based on τ–δ of linear ascending
$\Delta_{pa\text{-}\infty}$	slip at crack face for infinitely long element based on τ–δ of parabolic ascending
$\Delta_{pa\text{-}sp}$	slip at crack face for element length S_p based on τ–δ of parabolic ascending
$\Delta_{pa\text{-}sec}$	slip at crack face for element length $S_p/2$ based on τ–δ of parabolic ascending
$\Delta_{pa\text{-}sec}$	slip at crack face for element length $S_p/4$ based on τ–δ of parabolic ascending

use of FRP reinforcing bars in these empirical design rules as: FRP reinforcing bars have a very wide range of moduli E_r from 40 GPa to 140 GPa depending on the density of the fibre and the type of fibre such as GFRP, CFRP, and AFRP [14,2,4]; and furthermore, FRP reinforcing bars have a very wide range of bond characteristics depending on the manufacturing process such as reinforcing bar surfaces that are grain covered, ribbed, braided or smooth [14–18].

To help in the more rapid development and acceptance of FRP reinforced RC members, a mechanics based tension-stiffening approach [29] is used to quantify the deflection of RC flexural members with FRP reinforcing bars [19]. This mechanics based discrete rotation approach can be summarised as follows:

(1) Of fundamental importance is the bond–slip (τ/δ) characteristic between the reinforcement and the concrete.
(2) The bond–slip properties (τ/δ) are used directly to quantify the reinforcement-load crack-widening (P/Δ) relationship at a discrete crack which itself depends on the reinforcement FRP modulus.
(3) The (P/Δ) relationship is then used to determine the moment discrete rotation (M/θ) at each individual crack and consequently.
(4) From which the applied load deflection of a beam at serviceability can be determined.

Hence this mechanics based approach for the non time-dependent deflection of reinforced members can cope with any bond characteristic and any reinforcement modulus and consequently is ideally suited for RC members with FRP reinforcing bars.

This discrete rotation approach has been applied to steel reinforced RC beams and slabs and has been found to have good correlation with test results [20] when using the well established and accepted CEB model for the bond–slip characteristics [21] and in which the modulus of the steel reinforcement remains unchanged. In this paper, the discrete rotation approach is applied to a very wide range of FRP reinforcement moduli and a very wide range of FRP bond–slip characteristics at serviceability. To cater for the range of bond–slip properties, the discrete rotation deflection approach is given for both a serviceability linear ascending bond–slip characteristic and for a parabolic ascending bond–slip characteristic. The mechanics deflection model is then compared with FRP RC test results in which there is a variety of reinforcement moduli. Finally, the mechanics deflection model is used to illustrate the effects of varying the moduli and bond–slip charac-

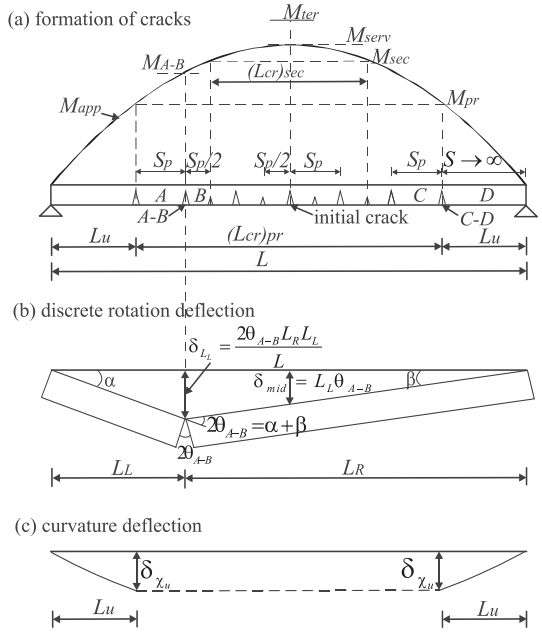

Fig. 1. Deflection of RC beam.

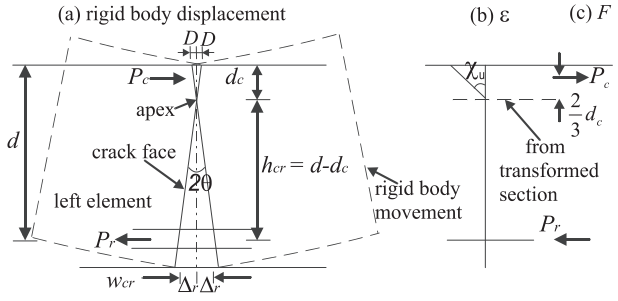

Fig. 2. Discrete rotation at a single crack.

teristics over the range currently available in FRP reinforcement not only on the deflection but also on the crack spacing and crack widths.

2. Discrete rotation deflection analysis

Consider the simply supported flexural member in Fig. 1a of span L in which the length of the cracked region is $(L_{cr})_{pr}$ and that of the uncracked region is $2L_u$. The member is subjected to an applied moment M_{app} that has a maximum moment of M_{serv}. The first crack to form in the beam in Fig. 1a is referred to as the *initial crack* and can be derived from the elementary moment–curvature beam theory of an uncracked section. After the initial crack has formed, the full-interaction moment–curvature approach can no longer be used to predict subsequent cracking. Instead the following partial-interaction discrete rotation approach [19] can be used.

2.1. Discrete rotation approach

The crack faces of the initial crack in Fig. 1a are assumed to rotate through a rigid body displacement as in Fig. 2a where the effective depth of the beam is d and where the crack apex, at h_{cr} from the tension reinforcement, can be determined from transformed sections.

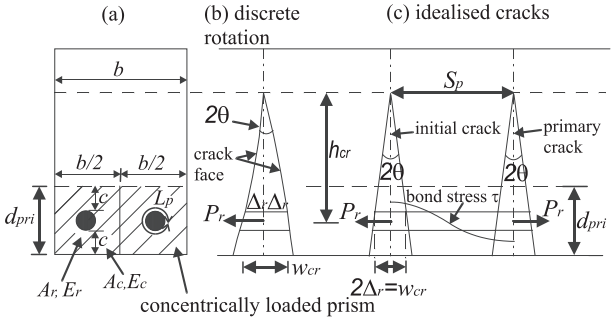

Fig. 3. Tension stiffening analysis.

The rigid body rotation in Fig. 2a induces a triangular deformation in the compression zone that has a maximum value of D as shown and, consequently, a linear variation in strain in the compression zone as in Fig. 2b. As this analysis is at serviceability, the concrete can be considered to remain linear elastic so the position of the resultant compressive force P_c in Fig. 2c is known. Furthermore, as the force in the tension reinforcement P_r in Fig. 2a depends on the slip of the reinforcement at the crack face Δ_r which depends on the bond–slip (τ/δ) properties, the force P_r can be determined, as will be shown later, so that the moment is

$$M_t = P_r\left(d - \frac{d_c}{3}\right) \tag{1}$$

The rotation of a crack face θ in Fig. 2a is directly proportion to the crack face slip Δ_r

$$\theta = \frac{\Delta_r}{h_{cr}} \tag{2}$$

and the width of the crack at the level of the reinforcement w_{cr} is equal to the sum of Δ_r at each crack face as shown.

It is common practise to determine the relationship between P_r and Δ_r in Fig. 2a from the partial-interaction tension stiffening analysis of concentrically loaded prisms of width $b/2$ and depth d_{pri} as in Fig. 3a and in which A_r and A_c and E_r and E_c are the cross-sectional areas and moduli of the reinforcement and concrete prism respectively and L_p is the bonded perimeter as shown [22–24,19]. The same partial-interaction analysis can used to determine the position S_p and reinforcement force P_r to cause cracking after the initial crack has formed, should the bond be strong enough, as illustrated in Fig. 3c. These subsequent cracks at spacing S_p are referred to as the primary cracks. The same analysis can also be used to predict when the concrete element of length S_p and depth d_{pri} between the crack faces in Fig. 3c cracks to form secondary cracks at a spacing of $S_p/2$, should the bond be strong enough. Furthermore if the bond is strong enough, to predict the formation of tertiary cracks at a crack spacing of $S_p/4$. These P/Δ relationships are given in the following sub-section for different bond–slip characteristics. Once the P/Δ relationship is known, the moment–rotation (M/θ) at a crack face can be determined from Eqs. (1) and (2).

2.2. Crack formation

After the initial crack has formed in Fig. 1a, the P/Δ analyses can be used to determine the force in the reinforcement to cause a primary crack F_{pr} (Eqs. (6) or (19) in the following sub-section depending on the bond–slip characteristics) and from Eq. (1) the moment to cause a primary crack M_{pr} in Fig. 1a. Hence, where the applied moment M_{app} in Fig. 1a exceeds M_{pr}, flexural cracks will form at a spacing S_p (Eqs. (9) or (20) over the region $(L_{cr})_{pr}$ as shown. The P/Δ analysis can also be used to determine the reinforcement force to cause secondary cracks F_{sec} (Eqs. (10) or (23))

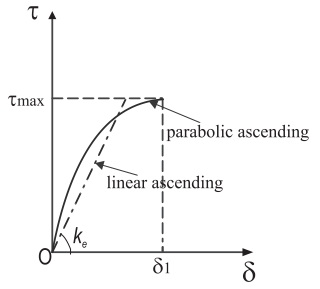

Fig. 4. Serviceability bond–slip.

and, consequently, the moment to cause secondary cracks M_{sec} and, consequently, the region $(L_{cr})_{sec}$ over which the cracks are spaced at $S_p/2$ (Eqs. (11) or (24)). The same can be done for tertiary cracks should the bond be strong enough for them to form. Hence the distribution of the flexural cracks in Fig. 1(a) can be determined.

2.3. Deflection due to discrete rotation

Having now formed the cracks as in Fig. 1a, the deflection due to the rotation of each individual crack within the cracked region $(L_{cr})_{pr}$ needs to be determined. For example, consider the crack marked *A–B* in Fig. 1a which is at a distance of L_L from the left support and in which the segment to the left marked *A* is of length S_p and that to the right marked *B* is of length $S_p/2$. The serviceability moment at that crack is M_{A-B} in Fig. 1a. Hence from Eq. (1) can be determined the reinforcement force P_r. This reinforcement force can be substituted into Eqs. (15) or (28), which are for an element of length S_p, for P_{sp} to derive the slip Δ_{sp} and from Eq. (2) the rotation of the left crack face. For the right crack face, the element has a length $S_p/2$ so that Eqs. (16) or (29) applies to derive the rotation of the right face. The sum of both of these rotations is $2\theta_{A-B}$ in Fig. 1b so that the contribution to the deflection of the beam from this individual crack is as shown in Fig. 1b. It can be seen from the geometry in Fig. 1b that from the rigid body displacement, the contribution of this crack to the mid-span deflection is simply $L_L\theta_{A-B}$.

For the crack marked *C–D* in Fig. 1a, no cracks form to the right so the element to the right marked *D* can be considered as infinitely long so that Eqs. (14) or (27) apply. It is simply a question of summing the deflections due to each individual crack to obtain the total deflection due to the discrete rotation of each individual cracks.

2.4. Deflection due to curvature

Outside the cracked region $(L_{cr})_{pr}$ in Fig. 1a that is within the uncracked regions of lengths L_u, the deflection can be visualised as that in Fig. 1c where the deflection due to curvature δ_χ can be derived by integrating the curvature over this uncracked region using the uncracked flexural rigidity. As an example, for a simply supported beam subjected to a uniformly distributed load, the length of the uncracked region L_u can be derived by solving the following equation

$$M_{pr} = -\frac{4M_{serv}}{L^2}\left(L_u^2\right) + \frac{4M_{serv}}{L}L_u \tag{3}$$

and the deflection due to curvature at L_u from the supports as shown in Fig. 1c is given by

$$\delta\chi_u = \frac{M_{pr}}{\left(L_uL - L_u^2\right)EI}\left(\frac{(L_u)^4}{4} - \frac{(L_u)^3L}{3}\right) \tag{4}$$

where *EI* is the flexural rigidity of the uncracked section.

3. P/Δ from linear ascending τ/δ characteristic

Two shapes of bond–slip characteristics will be considered in this serviceability analysis. The linear ascending bond–slip variation in Fig. 4 [19] which gives relatively simple closed form solutions and will be dealt with first. This is followed by the parabolic ascending characteristic which gives a range of bond slip properties that more closely resemble test results [16–18] but which give more complex closed form solutions. The equations required to determine the distribution of cracks will be given first and this is then followed by the equations required to determine the deflection for a given crack distribution. All the derivations of the fundamental equations have been given in Appendices A, B and C.

3.1. Linear-ascending bond–slip characteristic

The linear ascending bond–slip characteristic in Fig. 4 is given by

$$\tau = k_e\delta \tag{5}$$

where k_e is the stiffness as shown.

3.2. Linear ascending crack formation

The load in a reinforcing bar to induce a primary crack is given by

$$F_{li-pr} = \frac{A_rE_r\lambda_1^2f_{ct}A_c}{k_eL_p} \tag{6}$$

where as defined in Fig. 3a: A_r and E_r are the cross-sectional area and modulus of the FRP reinforcing bar; L_p is the perimeter length of the FRP bar; A_c is the cross-sectional area of the concentrically loaded prism; f_{ct} is the tensile strength of the concrete; and where

$$\lambda_1 = \sqrt{k_e\beta_2} \tag{7}$$

in which

$$\beta_2 = \frac{L_p}{A_r}\left(\frac{1}{E_r} + \frac{A_r}{E_cA_c}\right) \tag{8}$$

The primary crack spacing is given by

$$S_{li-pr} = \frac{2}{\lambda_1} \tag{9}$$

The load in the reinforcing bar to cause a secondary crack is given by

$$F_{li\_sec} = \frac{A_rE_r\lambda_1^2f_{ct}A_c}{0.35k_eL_p} \tag{10}$$

The secondary cracks occur midway between the primary cracks, so that the crack spacing in the region where secondary cracks occur, that is $(L_{cr})_{sec}$ in Fig. 1a, is half that of the primary crack spacing in Eq. (9), that is

$$S_{li-sec} = \frac{S_{li-pr}}{2} \tag{11}$$

The load in the reinforcing bar to cause a tertiary crack is given by

$$F_{li-ter} = \frac{A_rE_r\lambda_1^2f_{ct}A_c}{0.27k_eL_p} \tag{12}$$

which will cause the crack spacing to reduce to

$$S_{li-ter} = \frac{S_{li-pr}}{4} \tag{13}$$

3.3. Linear ascending deflection

The P/Δ relationships required to quantify the deflections are given below. They depend on the length of the prism being analysed.

When the prism length is greater than $S_{li\text{-}pr}$ as in region D in Fig. 1a, then the P/Δ relationship is given by

$$P_{li-\infty} = \Delta_{li-\infty} A_r E_r \lambda_1 \tag{14}$$

When the prism length is equal to $S_{li\text{-}pr}$ as in region C in Fig. 1a then

$$P_{li-sp} = \frac{\Delta_{li-sp} A_r E_r \lambda_1}{\tanh 2} \tag{15}$$

When the prism length is equal to $S_{li\text{-}pr}/2$ as in region B in Fig. 1a then

$$P_{li-sp/2} = \frac{\Delta_{li-sp/2} A_r E_r \lambda_1}{\tanh 1} \tag{16}$$

And finally when the prism length is equal to $S_{li\text{-}pr}/4$ then

$$P_{li-sp/4} = \frac{\Delta_{li-sp/4} A_r E_r \lambda_1}{\tanh 0.5} \tag{17}$$

4. P/Δ from parabolic ascending τ/δ characteristic

4.1. Parabolic bond–slip characteristic

The parabolic ascending bond–slip relationship in Fig. 4 is given by

$$\tau = \tau_{\max} \left(\frac{\delta}{\delta_1} \right)^{\alpha} \tag{18}$$

where δ_1 is the slip at the maximum shear stress τ_{max} as in Fig. 4 and α can be varied to match the shape with test results.

4.2. Parabolic ascending crack formation

The force in the reinforcing bar to cause a primary crack is

$$F_{pa-pr} = \frac{f_{ct}}{E_c} A_r E_r + f_{ct} A_c \tag{19}$$

The primary crack spacing is

$$S_{pa-pr} = \left[\frac{(1+\alpha) f_{ct} A_c \delta_1^{\alpha}}{\tau_{\max} L_p \left(\sqrt{2 c_9} \right)^{\alpha}} \right]^{\frac{1}{1+\alpha}} \tag{20}$$

where the coefficient c_9 can be derived from

$$c_9 - \frac{\sqrt{2 c_9} f_{ct} A_c \lambda_2 \delta_1^{\alpha}}{\tau_{\max} L_p} = -0.5 \left(\frac{f_{ct}}{E_c} + \frac{f_{ct} A_c}{A_r E_r} \right)^2 \tag{21}$$

in which

$$\lambda_2 = \frac{\beta_2 \tau_{\max}}{\delta_1^{\alpha}} \tag{22}$$

and in which β_2 is given by Eq. (8).

The force in the reinforcing bar to cause a secondary crack is

$$F_{pa-\sec} = A_r E_r \times \sqrt{\frac{2\lambda_2}{1+\alpha} (S_{pa-\sec})^{1+\alpha} \left(\frac{(1+\alpha) f_{ct} A_c \delta_1^{\alpha}}{\tau_{\max} L_p (S_{pa-\sec})^{1+\alpha}} \right)^{\frac{1+\alpha}{\alpha}} + \left(\frac{(1+\alpha) f_{ct} A_c \delta_1^{\alpha}}{\tau_{\max} L_p (S_{pa-\sec})^{1+\alpha}} \right)^{\frac{2}{\alpha}}} \tag{23}$$

where the spacing is now

$$S_{pa-\sec} = \frac{S_{pa-pr}}{2} \tag{24}$$

The force in the reinforcing bar to cause a tertiary crack is

$$F_{pa\_ter} = A_r E_r \times \sqrt{\frac{2\lambda_2}{1+\alpha} (S_{pa-ter})^{1+\alpha} \left(\frac{(1+\alpha) f_{ct} A_c \delta_1^{\alpha}}{\tau_{\max} L_p (S_{pa-ter})^{1+\alpha}} \right)^{\frac{1+\alpha}{\alpha}} + \left(\frac{(1+\alpha) f_{ct} A_c \delta_1^{\alpha}}{\tau_{\max} L_p (S_{pa-ter})^{1+\alpha}} \right)^{\frac{2}{\alpha}}} \tag{25}$$

and the spacing is now

$$S_{pa-ter} = \frac{S_{pa-pr}}{4} \tag{26}$$

4.3. Parabolic ascending deflection

The P/Δ relationships that are required for the deflection calculations depend on the prism encompassed by the cracks as follows.

When the prism length is greater than $S_{pa\text{-}pr}$ then

$$P_{pa-\infty} = A_r E_r \sqrt{\frac{2\lambda_2 \Delta_{pa-\infty}^{1+\alpha}}{1+\alpha}} \tag{27}$$

When the prism length equals $S_{pa\text{-}pr}$ then

$$P_{pa-sp} = A_r E_r \sqrt{\frac{2\lambda_2 \Delta_{pa-sp}^{1+\alpha}}{1+\alpha} + \left(\frac{\Delta_{pa-sp}}{S_{pa-pr}} \right)^2} \tag{28}$$

When the prism length $S_{pa\text{-}sec}$ equals $S_{pa\text{-}pr}/2$ then

$$P_{pa-sp/2} = A_r E_r \sqrt{\frac{2\lambda_2 \Delta_{pa-sp/2}^{1+\alpha}}{1+\alpha} + \left(\frac{\Delta_{pa-sp/2}}{S_{pa-\sec}} \right)^2} \tag{29}$$

and finally when the prism length $S_{pa\text{-}ter}$ equals $S_{pa\text{-}pr}/2$ then

$$P_{pa-sp/4} = A_r E_r \sqrt{\frac{2\lambda_2 \Delta_{pa-sp/4}^{1+\alpha}}{1+\alpha} + \left(\frac{\Delta_{pa-sp/4}}{S_{pa-ter}} \right)^2} \tag{30}$$

5. Validation

The discrete rotation deflection analysis described above for deriving the deflection has been compared with twelve specimens tested by [2] in Figs. 5–8. The simply supported beams had a span of 1.8 m, depth of 190 mm and those in Figs. 5 and 6 had a width of 160 mm and those in Figs. 7 and 8 a width of 140 mm. The specimens were tested with a constant moment region of 600 mm. All the specimens had GFRP reinforcing bars of modulus 60 GPa. The specimens in Figs. 5–8 are identified as *C-abc-Dx*, where: *abc* stands for the amount of reinforcement (for example, three bars of diameter 16 mm is 316); *x* stands for the cover of the GFRP bars (which for *D*1 is 20 mm and that for *D*2 is 40 mm); and *C*1 and *C*2 are the concrete properties which for *C*1 had a mean cylinder strength of 32.1 MPa and mean modulus of 25.7 GPa and for *C*2 a strength of 58.7 MPa and modulus of 26.0 GPa respectively. The pull tests to determine the bond–slip properties are reported [15] and show the linear ascending bond–slip characteristic in Fig. 4. From these results and allowing for the axial extension of the reinforcing bar on the measured slip, the bond–slip stiffness k_e was calculated as 43 N/mm^3. The test results in Figs. 5–8 have also been compared with the deflections from [8] and, furthermore, as we are dealing with a serviceability analysis, the load–deflections have been plotted at up to half the measured failure load.

The specimens in Figs. 5 and 6 had a cover of 40 mm so that the depth of the prism used in the analysis, that is d_{pri} in Fig. 3a, was either 92 mm or 96 mm. In these analyses, the discrete rotation

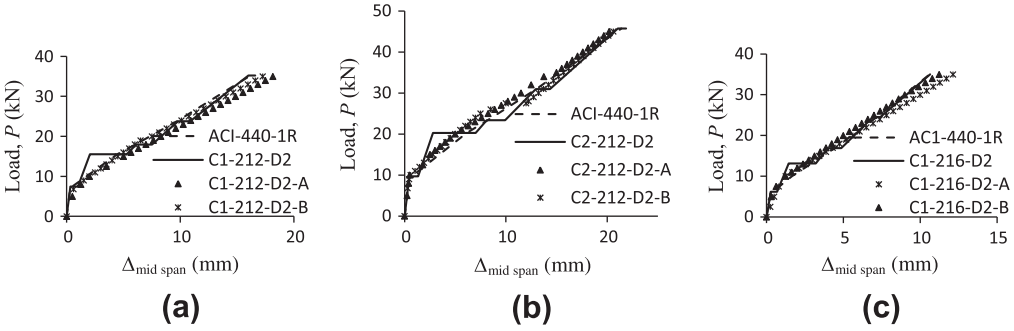

Fig. 5. Load mid span deflection for beams with cover of 40 mm.

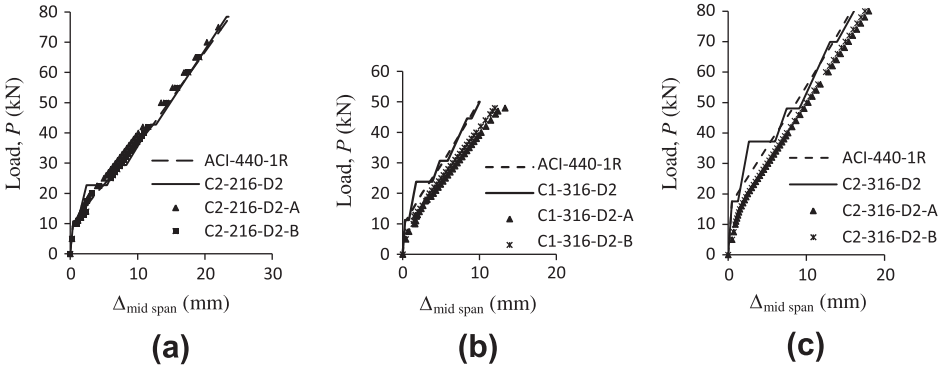

Fig. 6. Load–mid span deflection for beams with a cover of 40 mm.

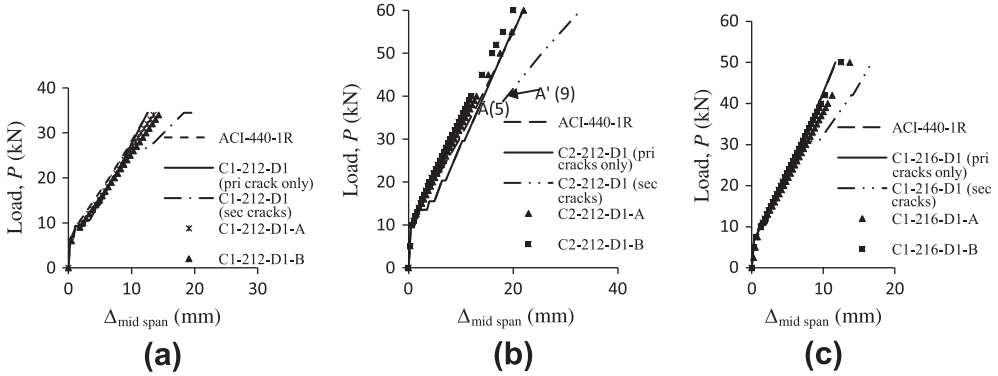

Fig. 7. Load–mid span deflection for beams with a cover of 20 mm.

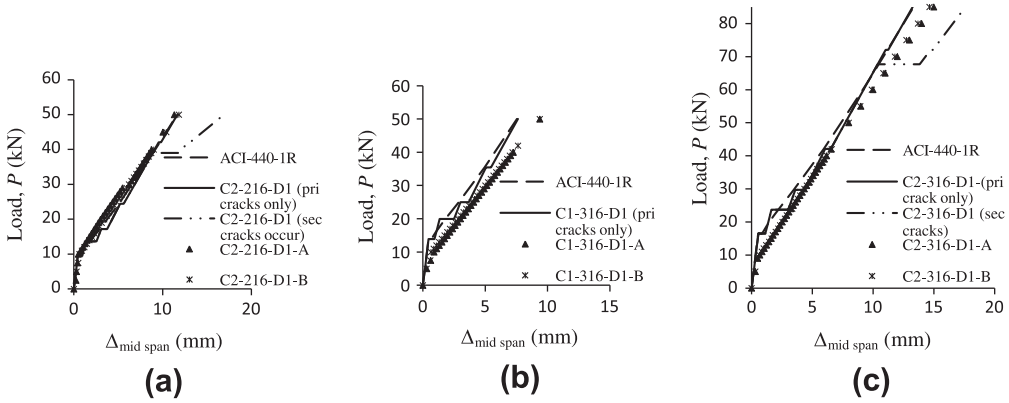

Fig. 8. Load–mid span deflection for beams with a cover of 20 mm.

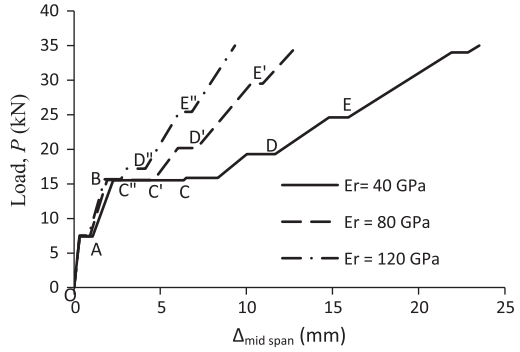

Fig. 9. Load mid-span deflection for varying E_r.

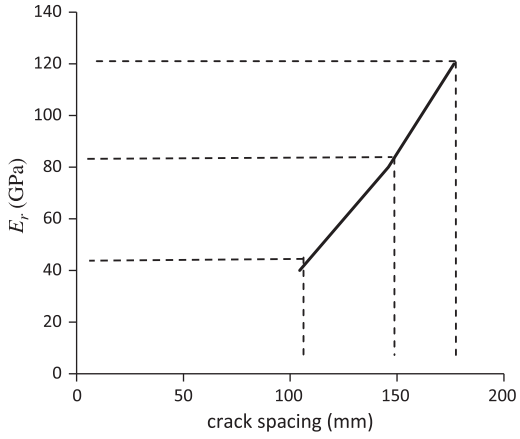

Fig. 10. Primary crack spacing for varying E_r.

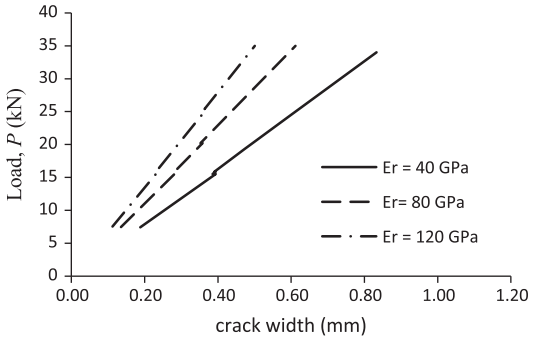

Fig. 11. Load crack width in constant moment region.

approach predicted that only primary cracks would occur and the step changes that can be seen are at the formation of additional primary cracks as the load is increased. In general, the theoretical discrete rotation approach would appear to have good correlation with the test results and in particularly with the ACI approach.

The specimens in Figs. 7 and 8 had a cover of 20 mm so that the depth of the prism used in the tension stiffening component of the analysis was either 52 mm or 56 mm. Hence in these specimens, the cross-sectional area of the prism A_c in Fig. 3a was about 57% of those in the specimens in Figs. 5 and 6. Let us first consider Fig. 7b. At the point marked $A(5)$, there are five primary cracks and then four secondary cracks form to cause the beam to deflect to $A'(9)$. This increase in deflection does not appear to occur in the tests specimens which would suggest that secondary cracks do not occur. If secondary cracks are suppressed in the discrete

Table 1
Bond–slip characteristic.

Type of outer surface	α	τ_{max} (MPa)	δ_1 (mm)	$S_{pa\text{-}pr}$ (mm)
Grain covered	0.067	12.05	0.13	40
Indented and braided	0.177	10.2	2.14	78
Ribbed type	0.283	11.61	1.23	81

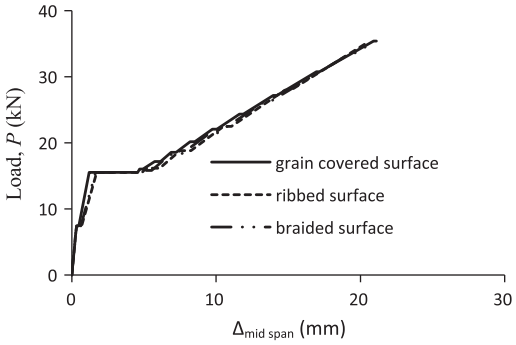

Fig. 12. Load–deflection with varying bond.

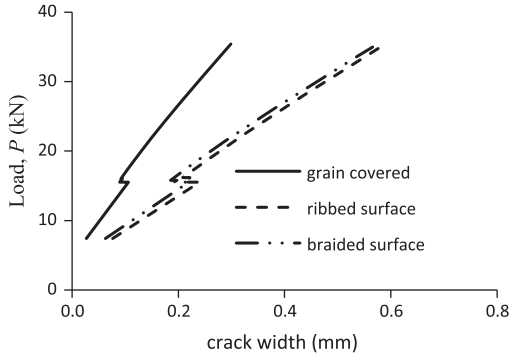

Fig. 13. Crack width with varying bond.

rotation analysis then there would appear to be continuing good correlation with the test results and the ACI approach in all of the specimens in Figs. 7 and 8. It would appear that the choice of A_c is important in determining the onset of secondary cracks.

The aim of this paper is to provide the mechanics tools for researchers to quantify the deflection of RC beams with any type FRP reinforcing bars and with any bond–slip characteristic. From the above comparisons, it would appear that a better estimate of A_c than that based on the cover would help as already exist [25].

6. Parametric study

The two major parameters that distinguish FRP RC from steel RC are the reinforcement moduli and the reinforcement bond–slip characteristics. Let us first consider the effect of varying the FRP reinforcement moduli on the deflection.

To illustrate the effect of varying the reinforcement moduli on the deflection, Specimen *C1-212-D2* in Fig. 5a was analysed with three values of E_r of 40 GPa, 80 GPa and 120 GPa; all other variables remained the same as those described in the previous section. The results are shown in Fig. 9. The first crack to form, which is referred to as the *initial crack* in Fig. 1a, occurs at load level *A* in Fig. 9 and can be determined from the standard moment–curvature analysis of an uncracked section. Hence in region *O–A* the deflection is purely due to curvature. In region *A–B*, the deflection is due to

curvature along the length of the beam and the discrete rotation of the single *initial crack*. The primary cracks first form at load level *B* in the constant moment region of the test specimen causing very large increases in the deflection, to *C*, *C′* and *C″*, due to discrete rotation of the cracks and which depends on the moduli of the reinforcement. At this stage most of the deflection is due to discrete rotation. The next primary cracks form at *D*, *D′* and *D″* outside the constant moment region and so on. It can be seen that the reinforcement moduli has a major effect on the deflection and mostly through the discrete rotation of the cracks.

The dependence of the primary crack spacing $S_{li\text{-}pr}$ on the reinforcement moduli can be determined from Eqs. (7)–(9) and is shown in Fig. 10; increasing the reinforcement moduli increases the crack spacing but not in a linear fashion. The effect of the reinforcement moduli on the average crack width in the constant moment region is shown in Fig. 11 where the reduction in the reinforcement moduli increases the deflection. In summary reducing the reinforcement moduli: increases crack spacing (Fig. 10) and therefore reduces the number of cracks and the points at which discrete rotation occurs; however this is offset by causing wider cracks (Fig. 11) and, therefore, greater discrete rotations at the cracks which do occur; with the net effect of greater deflections (Fig. 9).

To illustrate the effect of bond on the deflection due to the discrete rotation, the parabolic ascending bond–slip characteristic in Fig. 4 has been fitted to test results for grain covered, ribbed and indented and braided specimens [16]. The results are given in Table 1 where the bond slip exponent α and the slip δ_1 had very wide ranges for a fairly constant τ_{max}. Hence comparing deflection analyses with these results will be comparing the shapes of the bond–slip characteristics for fairly constant shear capacities τ_{max}. Specimen *C1-212-D2* was also used to illustrate the effect of the variation in bond on the deflection.

The load–deflection plots for Specimen *C1-212-D2* but with the different bond characteristics in Table 1 are shown in Fig. 12. It can clearly be seen that the bond properties have little effect on the deflection. The effect of the bond properties on the primary crack spacing $S_{pa\text{-}pr}$ is shown in Table 1 where it can be seen that it can cause large changes in the crack spacing. The effect of the bond on the average crack width in the constant moment region is shown in Fig. 13 where its effect can also be major. The step change at 15 kN where the average crack width in the constant moment region reduces is caused by cracking beyond the constant moment region which initially causes the cracks within the constant moment region to contract but it is worth noting the total crack width increases. In conclusion, the bond characteristics affect crack spacing and crack widths but have little effect on the deflection. For example, increasing the bond stiffness will reduce the crack spacing but this will be offset by narrower cracks so the effect on deflection is negligible.

7. Conclusions

This paper presents a mechanics approach for quantifying the serviceability discrete rotation of RC beams with FRP reinforcing bars in a generic form that will allow researchers to refine the components of the mechanics model to achieve close correlation with tests results. A partial-interaction discrete rotation mechanics based analysis for quantifying the short-term discrete rotation at cracks and consequently the deflection of RC beams with FRP reinforcement has been described. The model allows for the bond–slip characteristics between the reinforcement and the concrete and so can cope with any type of surface preparation of FRP reinforcing bars. The model also allows for the reinforcing bar force and slip at the crack face and so can cope with any type of FRP reinforcement model.

As part of the analysis procedure, the model also predicts the crack widening and crack spacing and the gradual development of discrete cracks such as initial, primary and secondary cracks should they occur. Hence the model can be used with any type of FRP reinforcement with any type of bond characteristics and is shown to have good agreement with test results. It may also be worth noting that individual cracks or concentrations of cracks continue to rotate causing very wide cracks which are often attributed to hinges and which may be further increased in size through concrete softening. Hence this research on the serviceability ductility is a precursor to the ultimate ductility of RC members.

Acknowledgements

This research was supported by the Australian Research Council Discovery grant DP0985828 "A unified reinforced concrete model for flexure and shear". The second author also thanks the Universiti Teknologi Malaysia and the Ministry of Higher Education of Malaysia for financial support.

Appendix A. Fundamental governing equation

The fundamental governing equation for basic tension stiffening can be derived from the equilibrium equations for any bonded joint such as a reinforced concrete prism under pure tension as shown in Fig. 14a. The derivation of the governing equation for this stress transfer problem involves four unknown fields which are: the axial stresses $\sigma_r = \sigma_r(x)$ in the reinforcement and $\sigma_c = \sigma_c(x)$ in the concrete; the axial strains $\varepsilon_r = \varepsilon_r(x)$ in the reinforcement and $\varepsilon_c = \varepsilon_c(x)$ in the concrete; the interface shear stress across the bonded length $\tau = \tau(x)$; and the interface slip $\delta = \delta(x)$ which is the difference between the axial displacement u_r of the reinforcement and u_c of the concrete [26–28].

From Fig. 14b and c, the generic equilibrium equations for a reinforced prism under pure tension can be written as

$$\frac{d\sigma_r}{dx} = \frac{\tau L_p}{A_r} \tag{A.1a}$$

and

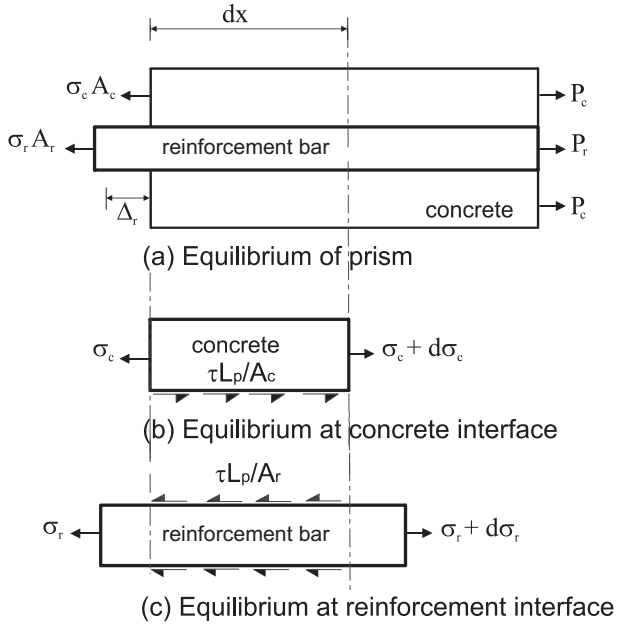

Fig. 14. Free body diagrams.

$$\frac{d\sigma_c}{dx} = -\frac{\tau L_p}{A_c} \tag{A.1b}$$

and from Fig. 14a, the equation of equilibrium for the prism can be written as

$$\sigma_c A_c + \sigma_r A_r = P_r \tag{A.2}$$

The axial tension force Pr in Eq. (A.2) will induce a slip at the interface (δ) between the concrete and reinforcement

$$\delta = u_r - u_c \tag{A.3}$$

Differentiating Eq. (A.3) gives the following slip strain $\frac{d\delta}{dx}$

$$\frac{d\delta}{dx} = \frac{du_r}{dx} - \frac{du_c}{dx} \tag{A.4}$$

As $\frac{du_r}{dx}$ is simply the reinforcement strain, from the steel and concrete moduli E_r and E_c respectively

$$\sigma_r = E_r \varepsilon_r = E_r \frac{du_r}{dx} \tag{A.5}$$

and

$$\sigma_c = E_c \varepsilon_c = E_c \frac{du_c}{dx} \tag{A.6}$$

where E_r and E_c are the elastic modulus of reinforcement and concrete respectively. Substituting Eqs. (A.5) and (A.6) into (A.4) yields

$$\frac{d\delta}{dx} = \frac{\sigma_r}{E_r} - \frac{\sigma_c}{E_c} \tag{A.7}$$

Differentiating Eq. (A.7), we get

$$\frac{d^2\delta}{dx^2} = \frac{1}{E_r}\left(\frac{d\sigma_r}{dx}\right) - \frac{1}{E_c}\left(\frac{d\sigma_c}{dx}\right) \tag{A.8}$$

and substituting Eqs. (A.1a) and (A.1b) into Eq. (A.8) yields the following governing equation

$$\frac{d^2\delta}{dx^2} - \beta_2 \tau = 0 \tag{A.9a}$$

where

$$\beta_2 = \frac{L_p}{A_r}\left(\frac{1}{E_r} + \frac{A_r}{E_c A_c}\right) \tag{A.9b}$$

The governing Eq. (A.9a) can be solved using the interfacial bond–slip characteristic $\tau = f(\delta)$ along with the boundary conditions for this specific tension stiffening problem. In this paper, the bond stress slip $\tau = f(\delta)$ in Fig. 4 has been used to derive the basic tension stiffening equations in the main text.

Appendix B. Derivation of basic tension stiffening for τ–δ of linear ascending

Solving the differential equation in Eq. (A.9a) which the bond stress slip of linear ascending τ–δ as shown in Fig. 4, gives

$$\delta(x) = c_1 \cosh(\lambda_1 x) + c_2 \sinh(\lambda_1 x) \tag{B.1}$$

and further differentiating Eq. (B.1) yields

$$\frac{d\delta}{dx} = \lambda_1 c_1 \sinh(\lambda_1 x) + \lambda_1 c_2 \cosh(\lambda_1 x) \tag{B.2}$$

and substituting the slip variation of Eq. (B.1) into the bond stress slip of linear ascending τ–δ will gives the bond stress variation

$$\tau(x) = k_e[c_1 \cosh(\lambda_1 x) + c_2 \sinh(\lambda_1 x)] \tag{B.3}$$

in which the constants c_1 and c_2 in the equations above can be solved through the substitution of boundary conditions as follows.

$$\frac{d\delta}{dx} = \frac{P_r}{A_r E_r} \text{ and } \delta = \Delta_r \text{ at } x = 0, \tag{B.4}$$

and

$$\delta = 0 \text{ and } \frac{d\delta}{dx} = 0 \text{ at } x = S_{li-pr} \tag{B.5}$$

where $S_{li\text{-}pr}$ in Eq. (B.5) is defined as a position beyond which the slip–strain tends to zero.

Solving both Eqs. (B.1) and (B.2) with applying the boundary conditions in Eqs. (B.4) and (B.5) yields

$$c_2 = \frac{P_r}{A_r E_r \lambda_1} \tag{B.6}$$

and

$$c_1 = -\frac{P_r}{A_r E_r \lambda_1 \tanh 2} \tag{B.7}$$

and $S_{li\text{-}pr}$

$$S_{li-pr} = \frac{2}{\lambda_1} \tag{B.8}$$

where $S_{li\text{-}pr}\lambda_1 = 2$ is based on an assumption that the bond stress is resisted by 97% of the applied load, P_r [28].

Relationship between the bond force and concrete force are shown below

$$\int_{x=0}^{x=S_p} \tau L_p \, dx = f_{ct} A_c \tag{B.9}$$

Substituting the variation of bond stress in Eq. (B.3) into Eq. (B.9) will gives the load in the reinforcing bar to cause a primary crack

$$F_{li-pr} = \frac{A_r E_r \lambda_1^2 f_{ct} A_c}{k_e L_p} \tag{B.10}$$

The boundary condition to form secondary crack spacing $S_{li\text{-}sec}$ is given by

$$\delta = 0 \text{ and } \frac{d\delta}{dx} \neq 0 \text{ at } x = S_{li-pr}/2 = S_{li-sec} \tag{B.11}$$

Solving Eq. (B.1) by using the boundary condition in Eq. (B.11) and constant of c2 in Eq. (B.6) gives

$$c_{1-\sec} = -\frac{P_r}{A_r E_r \lambda_1}(\tanh 1) \tag{B.12}$$

Thus the load in the reinforcing bar to induce secondary crack can be obtained through the substitution of Eqs. (B.12) and (B.6) into Eq. (B.3) and further into Eq. (B.9)

$$F_{li\_\sec} = \frac{A_r E_r \lambda_1^2 f_{ct} A_c}{0.35 k_e L_p} \tag{B.13}$$

The P–Δ relationship in Eqs. (15)–(17) in the main text can be derived through substitution of particular constants and the boundary conditions in Eq. (B.4) into Eq. (B.1). Let say, for P–Δ relationship of prism length that is equal to $S_{li\text{-}pr}$, substituting both constants of Eqs. (B.6) and (B.7) into (B.1) will gives

$$P_{li-sp} = \frac{\Delta_{li-sp} A_r E_r \lambda_1}{\tanh 2} \tag{B.14}$$

Appendix C. Derivation of basic tension stiffening for τ–δ of parabolic ascending

Substituting the bond stress of parabolic ascending into governing equation of Eq. (A.9a) leads to

$$\frac{d^2\delta}{dx^2} = \beta_2 \tau_{\max}\left(\frac{\delta}{\delta_1}\right)^{\alpha} \tag{C.1}$$

As

$$\frac{d^2\delta}{dx^2}=\frac{d}{dx}\left(\frac{d\delta}{dx}\right)=\frac{dv}{dx}=\frac{dv}{d\delta}\left(\frac{d\delta}{dx}\right)=v\frac{dv}{d\delta} \tag{C.2a}$$

where

$$v=\frac{d\delta}{dx} \tag{C.2b}$$

Eq. (C.1) can be rewritten as

$$v\frac{dv}{d\delta}=\beta_2\tau_{\max}\left(\frac{\delta}{\delta_1}\right)^{\alpha} \tag{C.3}$$

Integrating both sides of the equation yields

$$\frac{d\delta}{dx}=\sqrt{\frac{2\lambda_2\delta^{1+\alpha}}{1+\alpha}+2c_9} \tag{C.4}$$

and c_9 is a constant of integration.

Further integrating Eq. (C.4) yields

$$\delta\left(Hyp_2F_1\left[\frac{1}{2},\frac{1}{1+\alpha},1+\frac{1}{1+\alpha},-\frac{\lambda_2\delta^{1+\alpha}}{c_9}\right]\right)=(x+c_{10})\sqrt{2c_9} \tag{C.5}$$

where $Hyp2F1$ represents a $2F1$ hypergeometric function and it is a series of slip function. Solving that slip series functions in mathlab, an assumption has been made that this series is approximately 1.0 hence the slip variation in Eq. (C.5) can be rewritten as

$$\delta=(x+c_{10})\sqrt{2c_9} \tag{C.6}$$

For the boundary conditions of Eq. (B.5), in which $\delta = 0$ at $x = S_{pa\text{-}pr}$, the constant c_{10} in Eq. (C.6) can be obtained as

$$c_{10}=-S_{pa-pr} \tag{C.7}$$

Substituting Eq. (C.7) into the slip variation of Eq. (C.6) and further into the bond force and concrete force relationship of Eq. (B.9) gives the primary crack spacing

$$S_{pa-pr}=\left[\frac{(1+\alpha)f_{ct}A_c\delta_1^{\alpha}}{\tau_{\max}L_p\left(\sqrt{2c_9}\right)^{\alpha}}\right]^{\frac{1}{1+\alpha}} \tag{C.8}$$

Substituting the boundary conditions of Eq. (B.4) into Eqs. (C.4) and (C.6) will lead to the constant c_9

$$c_9-\frac{\sqrt{2c_9}f_{ct}A_c\lambda_2\delta_1^{\alpha}}{\tau_{\max}L_p}=-0.5\left(\frac{P_r}{A_rE_r}\right)^2 \tag{C.9}$$

where P_r is the load to cause the primary crack spacing $S_{pa\text{-}pr}$ that is $F_{pa\text{-}pr} = (f_{ct}/E_c)A_rE_r + f_{ct}A_c$

Thus the constant c_9 can be rewritten as

$$c_9-\frac{\sqrt{2c_9}f_{ct}A_c\lambda_2\delta_1^{\alpha}}{\tau_{\max}L_p}=-0.5\left(\frac{f_{ct}}{E_c}+\frac{f_{ct}A_c}{A_rE_r}\right)^2 \tag{C.10}$$

As the bar in the element is further pulled out, secondary cracks will occur. By symmetry, the secondary crack spacing $S_{pa\text{-}sec} = S_{pa\text{-}pr}/2$ and applying this boundary condition into (C.6) will leads to the constant c_{10_s}

$$c_{10\_s}=-S_{pa-\sec} \tag{C.11}$$

Substituting Eq. (C.11) into the slip variation of Eq. (B.11) and further into the bond force and concrete force relationship of Eq. (B.9) gives the constant c_{9_s}

$$c_{9\_s}=0.5\left[\frac{(1+\alpha)f_{ct}A_c\delta_1^{\alpha}}{\tau_{\max}L_p\left(S_{pa-\sec}\right)^{1+\alpha}}\right]^{\frac{2}{\alpha}} \tag{C.12}$$

Substituting the constant c_{9_s} and also Eq. (C.11) into the slip variation of Eq. (C.6) at $x = 0$ yields the following slip at the occurrence of the secondary crack for the prism of length $S_{pa\text{-}pr}$

$$\Delta_{r\_cr\_\sec}=S_{pa-\sec}\left(\frac{A_cf_{ct}\delta_1^{\alpha}(1+\alpha)}{\tau_{\max}L_p\left(S_{pa-\sec}\right)^{1+\alpha}}\right)^{\frac{1}{\alpha}} \tag{C.13}$$

Applying the boundary conditions of Eq. (B.4) and also Eq. (C.13) into Eq. (C.4) yields the following load to cause a secondary crack

$$F_{pa-\sec}=A_rE_r \times\sqrt{\frac{2\lambda_2}{1+\alpha}\left(S_{pa-\sec}\right)^{1+\alpha}\left(\frac{(1+\alpha)f_{ct}A_c\delta_1^{\alpha}}{\tau_{\max}L_p\left(S_{pa-\sec}\right)^{1+\alpha}}\right)^{\frac{1+\alpha}{\alpha}}+\left(\frac{(1+\alpha)f_{ct}A_c\delta_1^{\alpha}}{\tau_{\max}L_p\left(S_{pa-\sec}\right)^{1+\alpha}}\right)^{\frac{2}{\alpha}}} \tag{C.14}$$

For P–Δ relationship shows in Eq. (28), substituting the constants of Eq. (C.7) and the boundary conditions of (B.4) into Eqs. (C.4) and (C.6) yields

$$P_{pa-sp}=A_rE_r\sqrt{\frac{2\lambda_2\Delta_{pa-sp}^{1+\alpha}}{1+\alpha}+\left(\frac{\Delta_{pa-sp}}{S_{pa-pr}}\right)^2} \tag{C.15}$$

References

[1] Aiello MA, Ombres L. Load–deflection analysis of FRP reinforced concrete flexural members. ASCE, Compos Constr 2000;4(4):164–71.

[2] Barris C, Torres L, Turon A, Baena M, Catalan A. An experimental study of the flexural behaviour of GFRP RC beams and comparison with prediction models. J Compos Struct 2009:91, 286–295.

[3] Cosenza E, Greco C, Manfredi G, Realfonzo R. Flexural behaviour of concrete beams reinforced with fiber reinforced plastic (FRP) bars. In: Proc, 3rd int symp on non-metallic (FRP) reinforcement for concrete struct; 1997a. p. 463–70.

[4] Kassem C, Farghaly AS, Benmokrane B. Evaluation of flexural behaviour and serviceability performance of concrete beams reinforced with FRP bars. ASCE, Compos Constr 2011. http://dx.doi.org/10.1061/(ASCE)CC.1943-5614.0000216.

[5] Pecce M, Manfredi G, Cosenza E. Experimental response and code models of GFRP RC beams in bending. ASCE, Compos Constr 2000;6(3):154–61.

[6] Toutanji H, Saafi M. Flexural behaviour of concrete beams reinforced with glass fiber-reinforced polymer (GFRP) bars. ACI, Struct J 2000;97(5):712–9.

[7] Vogel H, Svecova D. New approach for estimating the deflection beams reinforced with FRP reinforcement. ASCE, Compos Constr 2008;6(12): 579–87.

[8] ACI Committee 440. Guide for the design and construction of concrete reinforced with FRP bars. Flamington Hills (US): ACI Publication; 2006.

[9] Bischoff PH, Gross SP. Design approach for calculating deflections of FRP reinforced concrete. ASCE, Compos Constr 2010. http://dx.doi.org/10.1061/(ASCE)CC.1943-5614.0000195.

[10] ACI Committee 318. Building code requirements for structural concrete. Detroit: ACI Publication; 2005.

[11] Bischoff PH. Deflection calculation of FRP reinforced concrete beams based on modifications to the existing Branson equations. ASCE, Compos Constr 2007;1(11):4–14.

[12] Branson DE. Instantaneous and time dependent deflections of simple and continuous reinforced concrete beams. HPR rep. no. 7, Alabama Highway Dept. Bureau of Public Roads; 1965.

[13] Castel A, Vidal T, Francois R. Effective tension active cross-section of reinforced concrete beams after cracking. Mater Struct 2006;39:115–26.

[14] Aiello MA, Leone M, Pecce M. Bond performances of FRP rebars-reinforced concrete. ASCE, Mater Civ Eng 2007;19(3):205–13.

[15] Baena M, Torres L, Turon A, Barris C. Experimental study of bond behaviour between concrete and FRP bars using a pull-out test. J Compos Part B 2009;40:784–97.

[16] Cosenza E, Manfredi G, Realfonzo R. Behaviour and modeling of bond of FRP rebars to concrete. ASCE, Compos Constr 1997;1(2):40–51.

[17] Pecce M, Manfredi G, Realfonzo R, Cosenza E. Experimental and analytical evaluation of bond properties of GFRP bars. ASCE, Mater Civ Eng 2001;13(4): 282–90.

[18] Rossetti VA. Local bond stress–slip relationships of glass fiber reinforced plastic bars embedded in concrete. Mater Struct 1995;28:340–4.

[19] Muhamad R. The tension stiffening in reinforced concrete beams and slabs. PhD thesis 2011. University of Adelaide., Adelaide, Australia; 2011.

[20] Muhamad R, Oehlers DJ, Mohamed Ali MS. Discrete rotation deflection of RC beams at serviceability. ICE Struct Build 2011. http://dx.doi.org/10.1680/stbu.2011.164.1.1.

[21] CEB. CEB model code 90. London; 1992.

[22] Jiang DH, Shah SP, Andonian AT. Study of the transfer of tensile forces by bond. J Am Concr Inst 1984;81(3):251–9.

[23] Gupta AK, Maestrini SR. Tension stiffening model for reinforced concrete bars. J Struct Eng 1990;16(3):769–90.

[24] Marti P, Alvarez M, Kaufmann W, Sigrist V. Tension chord model for structural concrete. Struct Eng Int 1998;8(4):287–98.

[25] CEB. CEB-FIP model code 2010. London: Thomas Telford; 2010.

[26] Mohamed Ali MS, Oehlers DJ, Griffith MC, Seracino R. Interfacial stress transfer of near surface-mounted FRP-to-concrete joints. Eng Struct 2008;30(7): 1861–8.
[27] Muhamad R, Mohamed Ali MS, Oehlers DJ, Sheikh AH. Load–slip relationship of tension reinforcement in reinforced concrete members. Eng Struct 2011;33(4):1098–106.
[28] Yuan H, Teng JG, Seracino R, Wu ZS. Full range behaviour of FRP-to-concrete bonded joints. Eng Struct 2004;26(5):543–691.
[29] Muhamad R, Mohamed Ali MS, Oehlers DJ, Griffith MC. The tension stiffening mechanism in reinforced concrete prisms. Int J Adv Struct Eng, accepted for publication.